Optimality in the Development of Intestinal Crypts

Shalev Itzkovitz,[1,2] Irene C. Blat,[2,3] Tyler Jacks,[2,3,4] Hans Clevers,[5] and Alexander van Oudenaarden[1,2,3,5,*]
[1]Department of Physics
[2]Department of Biology
[3]Koch Institute for Integrative Cancer Research
[4]Howard Hughes Medical Institute
Massachusetts Institute of Technology, Cambridge, MA 02139, USA
[5]Hubrecht Institute-KNAW (Royal Netherlands Academy of Arts and Sciences) and University Medical Center Utrecht, Uppsalalaan 8, 3584 CT Utrecht, Netherlands
*Correspondence: avano@mit.edu
DOI 10.1016/j.cell.2011.12.025

SUMMARY

Intestinal crypts in mammals are comprised of long-lived stem cells and shorter-lived progenies. These two populations are maintained in specific proportions during adult life. Here, we investigate the design principles governing the dynamics of these proportions during crypt morphogenesis. Using optimal control theory, we show that a proliferation strategy known as a "bang-bang" control minimizes the time to obtain a mature crypt. This strategy consists of a surge of symmetric stem cell divisions, establishing the entire stem cell pool first, followed by a sharp transition to strictly asymmetric stem cell divisions, producing nonstem cells with a delay. We validate these predictions using lineage tracing and single-molecule fluorescence in situ hybridization of intestinal crypts in infant mice, uncovering small crypts that are entirely composed of Lgr5-labeled stem cells, which become a minority as crypts continue to grow. Our approach can be used to uncover similar design principles in other developmental systems.

INTRODUCTION

Renewing mammalian tissues exhibit a hierarchical division into stem cells, immortal nondifferentiated cells with unlimited self-renewing capacity, and shorter-lived, more differentiated progenies (Moore and Lemischka, 2006; Slack, 2000; van der Flier and Clevers, 2009). Such architecture can be seen in the epithelium of the intestine (Potten and Loeffler, 1990; van der Flier and Clevers, 2009), the skin (Blanpain and Fuchs, 2006), the olfactory system (Lander et al., 2009), and in the hematopoietic system (Morrison et al., 1995b).

The stem cell hierarchy provides tissues with several advantages. One is a spatial segregation of stem cells in distinct niches (Moore and Lemischka, 2006; Watt and Hogan, 2000). These niches physically protect stem cells from the hostile tissue environment and provide signaling cues that are essential for their maintenance. Another advantage is the unique capacity of stem cells to modulate their modes of division. Stem cells can divide symmetrically, yielding either two stem cell or two nonstem cell progenies. Alternatively, stem cells can divide asymmetrically, yielding one stem cell progeny and another progeny destined for differentiation. Whereas asymmetric stem cell divisions maintain stem cell numbers, symmetric stem cell divisions facilitate the developmental growth of the stem cell compartment, as well as the regeneration of the stem cell pool following injury (Lander et al., 2009). Thus the ability of stem cells to divide either symmetrically or asymmetrically provides tissues with a flexibility to dynamically control the tissue composition in face of perturbations. This proliferative flexibility also carries with it a risk—insufficient proliferation deprives the tissue of the necessary flux of differentiated cells, whereas excessive divisions could result in pathological outgrowths (Lander et al., 2009). Thus the rates and modes of stem cell proliferation must be tightly controlled during adult life.

Several studies based on mathematical modeling have yielded important insights into the proliferative dynamics of adult mammalian stem cells. Simons and coworkers analyzed clone size distributions in different mouse tissues to infer the extent at which stem cells divide symmetrically (Clayton et al., 2007; Klein et al., 2010; Lopez-Garcia et al., 2010; Snippert et al., 2010). Other studies inferred the rates of symmetric stem cell divisions in human intestinal crypts from heterogeneity of methylation patterns (Yatabe et al., 2001). Theoretical modeling suggested that the size and dynamics of the adult intestinal stem cell pool might be optimal for minimizing the risk of cancer (Frank et al., 2003; Michor et al., 2003). Lander et al. (2009) used feedback control theory to explore how stem cell proliferation can robustly maintain homeostasis in face of perturbations (Reeves and Fraser, 2009). Loeffler and colleagues recently developed a comprehensive mathematical model that reconstructs the spatial patterns of proliferation and differentiation as well as the clonal dynamics in adult crypts (Buske et al., 2011). Less attention has been given to the cell dynamics during early development of tissues that rely on stem cells for their maintenance later in adulthood. In this study, we use optimal control theory to explore the design principles of the development of

a classic model system for adult stem cells—the mouse intestinal crypts.

The mouse small intestine constitutes one of the best-studied model systems for mammalian stem cell biology (Potten and Loeffler, 1990; van der Flier and Clevers, 2009). The small intestine is lined with a single layer of epithelial cells, which form crypts—invaginations into the underlying connective tissue. Stem cells reside at a designated niche at crypt bases and continuously proliferate throughout adult life. The direct progenies of stem cells, termed ''transit-amplifying'' cells, migrate up along the crypt axis as they divide several more times. These progenies eventually differentiate into either enterocytes, cells that absorb nutrients, or several different types of secretory cells. The differentiated postmitotic cells continue their migration along the finger-like villi that protrude into the lumen and are eventually shed from the villi tips (Potten and Loeffler, 1990; van der Flier and Clevers, 2009). The arrangement of stem cells and differentiated progenies in spatially distinct compartments and the availability of robust markers for stem cell identification (Barker et al., 2007) has made the murine intestinal crypt an ideal model system to study the homeostasis of stem cell-maintained tissues.

The epithelium in newborn mice lacks crypts but contains villi with differentiated cells, formed during late embryogenesis, that are able to sustain the digestive activity for the first days after birth (Al-Nafussi and Wright, 1982; Schmidt et al., 1988). However, these cells are short lived and it is essential for the young mouse to rapidly develop the functional crypt-villus structure to ensure a constant supply of enterocytes and secretory cells. This timing challenge imposes strict conditions on the dynamics of crypt development. Shortly after birth, small crypts begin to bud out from the intervillus pockets and rapidly increase in size. Crypt growth entails the addition of stem cells and nonstem cells toward the proportions seen in an adult crypt. The dynamics of stem cell proportions during this process, which fundamentally affect both timing and composition of growing crypts, have thus far not been characterized.

Here we seek design principles (Alon, 2006) that govern this crypt morphogenetic process. We explore how the choices that stem cells dynamically make between symmetric and asymmetric divisions determine the dynamic crypt composition, as well as the time to achieve a mature crypt. We use optimal control theory to show that a unique stem cell proliferation choice attains a mature crypt at the minimal possible time. This choice gives rise to a temporal order in which the entire stem cell pool is established first via symmetric stem cell divisions, followed by a sharp transition to asymmetric divisions, expanding the nonstem cells at a delay. We experimentally verify this behavior using sensitive in situ detection of the Lgr5 intestinal stem cell marker, and lineage tracing of the progenies of Lgr5 cells.

RESULTS

Stem Cell Proliferation Strategies Determine the Dynamics of Crypt Development

To begin to analyze the dynamics of crypt development we considered hypothetical crypt lineage histories (Figure 1). We first assume that a crypt stem cell can either divide symmetrically yielding an additional stem cell, or asymmetrically, yielding an additional nonstem cell progeny (Clayton et al., 2007; Lopez-Garcia et al., 2010; Morrison and Kimble, 2006; Potten and Loeffler, 1990; Snippert et al., 2010; Yatabe et al., 2001). Later we will relax this assumption and analyze an extension that considers also symmetric divisions into two nonstem cell progenies. Nonstem cell progenies, termed transit-amplifying cells continue to divide while migrating along the crypt axis until eventually being extruded from the crypt. The choice that stem cells make between symmetric and asymmetric divisions dynamically controls the relative proportions of stem cells and nonstem cells in the developing crypts. Purely asymmetric divisions rapidly expand the nonstem cell pool while maintaining a small constant number of stem cells (Figures 1A and 1D). Balanced strategies consisting of both symmetric and asymmetric divisions can give rise to crypts with constant proportions of stem cells and nonstem cells (Figures 1B and 1E). Another strategy entails a surge of symmetric divisions, rapidly expanding the stem cell pool, followed by a transition to asymmetric divisions, expanding the nonstem cell pool with a delay (Figures 1C and 1F). Thus stem cell proliferation strategies can achieve different desired goals, such as rapid generation of either stem cells or nonstem cells, or fixed proportions of these cell types throughout the process.

The availability at birth of differentiated cells able to sustain the digestive activity for ~10–14 days (Al-Nafussi and Wright, 1982; Schmidt et al., 1988) provides a time window during which a crypt can be established without the need to supply the tissue with the required differentiated cells. But because the hostile intestinal environment is detrimental to differentiated epithelial cells, a physiologically relevant optimization goal would be to minimize the time to achieve a mature crypt. In the mature crypts the stem cell and transit-amplifying pools continuously generate differentiated cells that live for a shorter time (typically 3–5 days [Potten and Loeffler, 1990; van der Flier and Clevers, 2009]) thus minimizing the accumulated damage for each individual cell. Consistent with the assumption that the tissue is optimized to establish crypts as fast as possible, the overall proliferation rates of epithelial cells during crypt morphogenesis have been shown to be significantly higher than in the adult mouse (Thrasher and Greulich, 1965). It is not immediately obvious which stem cell proliferation strategy would be optimal to achieve this goal. Early expansion of nonstem cells (Figure 1A) could be advantageous as it rapidly produces nonstem cells, which form the majority in the mature crypt. Alternatively, fast maturation of intestinal crypts could also be achieved by either balanced production of both cell types (Figure 1B) or early expansion of stem cells (Figure 1C). This last strategy would introduce long-lived cells with the capacity to further expand nonstem cells in the future while delaying nonstem cell production. The manner in which intestinal stem cells behave to form a mature crypt can be formalized as a minimal time problem under the framework of optimal control theory.

Optimal Control Theory Predicts that "Bang-Bang" Control of Stem Cell Proliferation Minimizes Time to a Mature Crypt

Optimal control theory considers processes in which a control function dynamically affects the evolution of state variables to achieve a desired goal. This theory has been extensively used

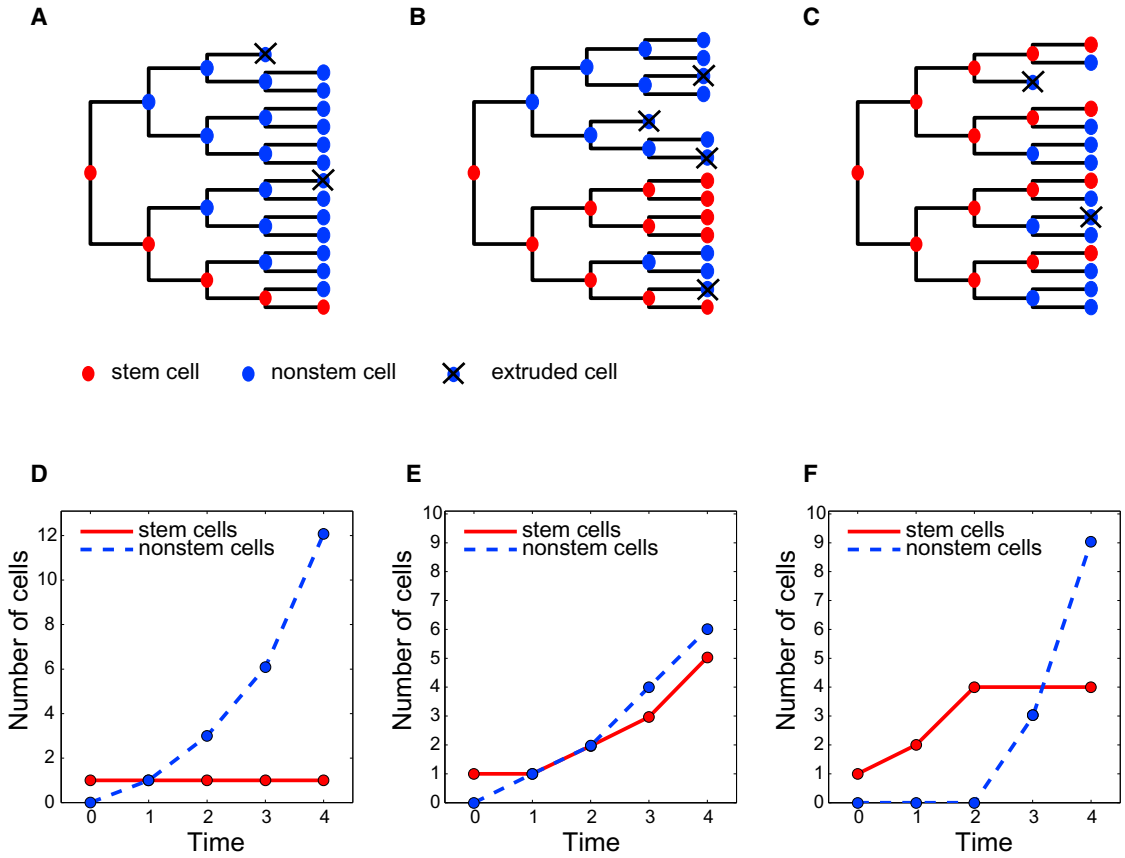

Figure 1. Stem Cell Division Strategies Determine Dynamic Crypt Composition

Hypothetical lineage trees (A–C) and resulting cell type dynamics (D–F) for purely asymmetric stem cell division (A and D), mixed symmetric and asymmetric divisions (B and E) and symmetric divisions transitioning to asymmetric divisions (C and F). Stem cells are red, nonstem cells are blue and extruded cells are marked with X.

in economics and engineering (Kirk, 2004; Koo, 1977). Previous applications of optimal control theory in biology included an analysis of the response of the immune system to an antigen (Perelson et al., 1976), mutation rates in cancer (Komarova et al., 2008) and reproduction strategies of social insects (Macevicz and Oster, 1976). This latter problem, which has some similarities with the crypt developmental problem, considered the optimal choice that queen wasps dynamically make throughout a reproductive season between producing workers, which increase the nest's resources but do not reproduce, and reproductive nonworking progeny, with the aim of maximizing the reproductive progeny at the end of the season (Macevicz and Oster, 1976).

In the crypt developmental process, the state variables are the numbers of stem cells $n(t)$ and nonstem cells $N(t)$ (Figures 2A and 2B). The goal is to increase these numbers from a given initial state (n_0,N_0) to the state found in a mature crypt (n_T,N_T) at the minimal possible time T. The numbers of stem cells and nonstem cells dynamically evolve according to the following differential equations (Figures 2A and 2B):

$$\frac{dn(t)}{dt} = \beta_n\, p(t) n(t) \qquad (1)$$

$$\frac{dN(t)}{dt} = \beta_n [1 - p(t)] n(t) + (\beta_N - \alpha) N(t) \qquad (2)$$

Stem cells and nonstem cells divide with rates β_n and β_N, respectively. Importantly, however, unlike stem cells that are anchored at the crypt bottoms and (in the absence of cell death) remain within the crypts indefinitely, nonstem cells are removed at a rate, α, mainly as a result of extrusion from crypts due to upward migration (Grey, 1968; Schmidt et al., 1988). For simplicity, we first assume that the extrusion rate is constant throughout the process, and later show that the results are insensitive to this assumption (Supplemental Information available online). The numbers of both stem cells and nonstem cells is governed by the probability $p(t)$ that a stem cell divides symmetrically into two stem cells at each time point. This probability is the control function of the process. The space of possible functions is huge, and analytical methods are therefore essential. By solving this optimality problem, we can discern which particular function can achieve the required crypt at the minimal possible time.

We used Pontryagin's minimum principle (Kirk, 2004) to solve the minimal time problem of crypt development (Figure 2 and Supplemental Information). The optimal solution includes two distinct phases—one in which all stem cells divide symmetrically,

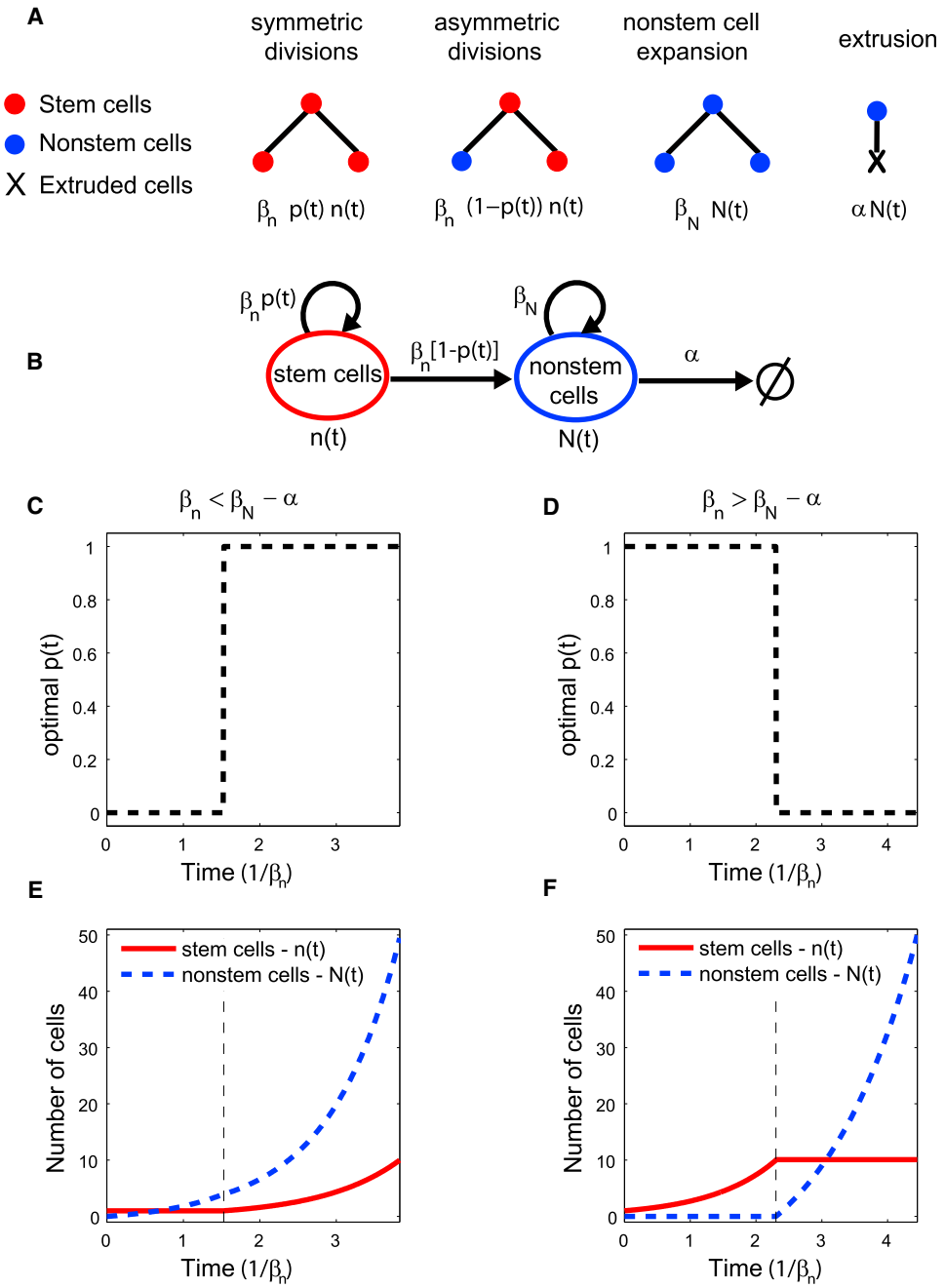

Figure 2. Bang-Bang Control Solution for Minimizing the Time to Attain a Mature Crypt

(A) Rates of change in the numbers of stem cells, $n(t)$ and nonstem cells, $N(t)$ as a function of the proliferation rates β_n, β_N, the extrusion rate α, and the probability that a stem cell divides symmetrically into two stem cells, $p(t)$.

(B) State diagram describing the dynamics of developing crypts.

(C) The optimal strategy when the yield of nonstem cells per asymmetrically dividing stem cell is lower than that from a nonstem cell ($\beta_n < \beta_N - \alpha$) entails initial asymmetric stem cell divisions of all stem cells followed by a transition to symmetric divisions. This optimal control gives rise to an early increase in nonstem cells and a delayed production of additional stem cells (E).

(D) The optimal strategy when the yield of nonstem cell per asymmetrically dividing stem cell is higher than that from a nonstem cell ($\beta_n > \beta_N - \alpha$) entails initial symmetric divisions of all stem cells followed by a transition to asymmetric divisions. This optimal control gives rise to an initial expansion of the entire stem cell pool and a delayed production of nonstem cells (F).

(E and F) show the resulting dynamics of stem cell and nonstem cell numbers for the optimal solutions of (C,D) respectively. Parameters used are $n_0 = 1$, $N_0 = 0$, $n_T = 10$, $N_T = 50$, $\beta_N - \alpha = 1.1 \times \beta_n$ (C,E) $\beta_N - \alpha = 0.7 \times \beta_n$ (D,F). See also Figure S1.

increasing their numbers exponentially, and a second phase during which all stem cells divide asymmetrically, maintaining their numbers while generating the nonstem cell progenies. Thus mixed strategies, in which some stem cells divide symmetrically whereas others divide asymmetrically (Figure 1B), are nonoptimal. For the optimal solution all stem cells divide identically at each time point, either symmetrically ($p(t) = 1$) or asymmetrically ($p(t) = 0$). Such a strategy in which the control function achieves its extreme value at any given time is termed a bang-bang control (Macevicz and Oster, 1976; Perelson et al., 1976). The sequence of these phases depends on the relation between the yield of nonstem cells per dividing nonstem cell, $\beta_N - \alpha$, and the yield per asymmetrically dividing stem cell, β_n (Equation 2, Figure 2B). If $\beta_n < \beta_N - \alpha$ asymmetrically dividing stem cells produce nonstem cells at a lower rate compared to dividing nonstem cells. In this regime, the optimal solution entails expansion of the nonstem cell pool first, followed by a transition to symmetric expansion of the stem cell pool (Figures 2C and 2E). Alternatively, if $\beta_n > \beta_N - \alpha$, expansion of the entire stem cell pool via symmetric stem cell divisions precedes a transition to nonstem cell production (Figures 2D and 2F). Equations 1 and 2 indicate that mature crypts would be obtained at the shortest time if the proliferation rates of both stem cells and nonstem cells would be set at their highest possible values ($\beta_n = \beta_N = \beta_{max}$), where β_{max} is a maximal proliferation rate that is consistent with other constraints such as maintaining the fidelity of DNA replication. In this regime $\beta_n > \beta_N - \alpha$ and a minimal time to a mature crypt entails expansion of the entire stem cell pool, followed by the creation of nonstem cells (Figures 2D and 2F; Figure S1). The transition time τ between the symmetric and asymmetric phases can be analytically solved (Supplemental Information). When $\beta_n > \beta_N - \alpha$ it depends only on the initial and final numbers of crypt stem cells and on their proliferation rate, $\tau = \ln(n_T/n_0)/\beta_n$.

Mature Crypts Can Be Achieved More Rapidly if Stem Cell Numbers Overshoot

Our optimal control model has so far considered only two modes of stem cell divisions—asymmetric divisions yielding a stem cell and a nonstem cell and symmetric divisions into two stem cell progenies. We next asked how the optimal solution would change if stem cells could also divide symmetrically into two nonstem cells during the developmental process (Figure 3). Such symmetric divisions have been shown to be ubiquitous in both adult murine intestinal crypts (Snippert et al., 2010) as well as in human crypts (Yatabe et al., 2001). We considered the following proliferation events: a stem cell division into two stem cells with probability $p(t)$, into two nonstem cells with probability $q(t)$ and into one stem cell and one nonstem cell with probability $1 - p(t) - q(t)$ (Figure 3A). The new state equations are:

$$\frac{dn(t)}{dt} = [p(t) - q(t)]\beta_n n(t) = p'(t)\beta_n(t)n(t) \quad (3)$$

$$\begin{aligned}\frac{dN(t)}{dt} &= [1 - p(t) - q(t)]\beta_n n(t) + 2\beta_n q(t)n(t) + (\beta_N - \alpha)N(t) \\ &= [1 - p'(t)]\beta_n n(t) + (\beta_N - \alpha)N(t)\end{aligned} \quad (4)$$

Where $p'(t) = p(t) - q(t)$ is the effective symmetric probability. Strikingly these equations are identical to the state equations of the basic model that excluded symmetric stem cell divisions into two nonstem cell progenies (Equations 1 and 2). The control function $p'(t)$ is now bounded by $-1 \leq p'(t) \leq 1$, as opposed to $0 \leq p(t) \leq 1$. If stem cell numbers are only allowed to increase during the process $0 \leq p'(t) \leq 1$ (Equation 3) and the extended model is identical to the basic model. The bang-bang control therefore remains the optimal solution. Notably, however, the control function $p'(t)$ no longer represents the probability that any individual stem cell divides symmetrically. This function can now include many combinations of the single-cell symmetric probabilities $p(t)$ and $q(t)$ (Figure 3), and thus the asymmetric phase ($p'(t) = 0$) could be comprised of all stem cells dividing strictly asymmetrically ($q(t) = p(t) = 0$), or alternatively any combination of two equal groups of stem cells, one group composed of stem cells dividing symmetrically into two stem cells and the other of stem cells dividing symmetrically into two nonstem cells ($q(t) = p(t) > 0$).

Interestingly, if the probability that a stem cell divides into two nonstem cells is allowed to exceed the probability to divide into two stem cells ($q(t) > p(t)$), (Figures 3B and 3D) a mature crypt can be attained in a shorter time compared to the optimal solution when $q(t) \leq p(t)$ (Figures 3C and 3E). In this solution, all stem cells divide symmetrically to increase their numbers until the very last developmental generation. In the last generation the majority of stem cells divide symmetrically into nonstem cells and the rest divide symmetrically into stem cells (Figures 3B and 3D). Thus if stem cell numbers overshoot the numbers required in the adult crypt, a mature crypt can be achieved more rapidly.

Single-Molecule FISH Enables Tracking the Dynamics of Lgr5 Stem Cells throughout the Developmental Process

To test the predictions of our optimality model we performed single-molecule fluorescence in situ hybridization (FISH) (Itzkovitz et al., 2011; Raj et al., 2010, 2008) on intestinal frozen sections harvested from infant mice with the stem cell marker Lgr5 (Figures 4, 5, and 6; Figure S2). The Lgr5 gene has been shown to be a specific stem cell marker expressed in a confined spatial location at the very bottom of intestinal crypts (Barker et al., 2007). Recent work demonstrated that in the adult crypts all Lgr5 cells have equal stem cell potential (Snippert et al., 2010). Thus, the number of Lgr5-positive cells can serve as a proxy for the number of crypt stem cells. To examine whether Lgr5 also marks stem cells during crypt development we performed long-term lineage tracing of Lgr5 progenies in infant *Lgr5-EGFP-IRES-CreERT2*, *Rosa26*$^{LSL\text{-}LacZ}$ mice (Barker et al., 2007). We detected ubiquitous labeled ribbons of lacZ-stained Lgr5 cell progenies extending from the bottoms of the crypts to the villi 9 days (Figure S2A) and 4 weeks (Figure 4A) after tamoxifen injection, establishing that Lgr5 also marks crypt stem cells during crypt morphogenesis.

Single-molecule FISH, which has previously been successfully applied in *Caenorhabditis elegans* and *Drosophila* tissues (Raj et al., 2010, 2008) as well as in mouse intestinal tissue (Itzkovitz et al., 2011), is based on the hybridization of multiple singly labeled probes that are complementary to a gene of interest, revealing mRNA molecules as diffraction limited spots

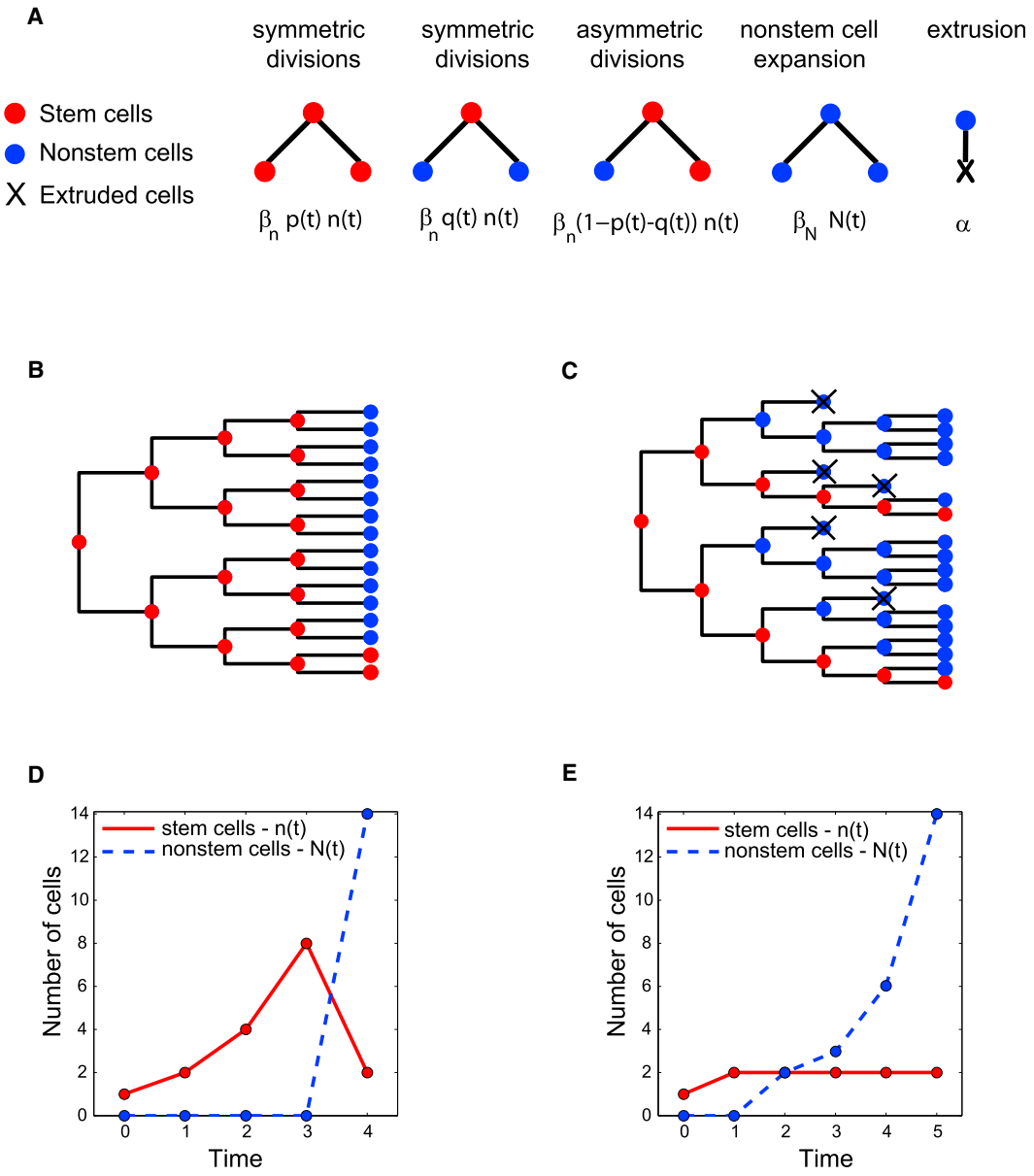

Figure 3. A Mature Crypt Can Be Achieved More Rapidly if Stem Cell Numbers Are Allowed to Overshoot

(A) Stem cell dynamics in a model that includes both symmetric divisions into two stem cells (with probability $p(t)$) and symmetric divisions into two nonstem cells (with probability $q(t)$).

(B–E) Example of a mature crypt, containing two stem cells and 14 nonstem cells, which can be obtained in a shorter time if stem cell numbers are allowed to overshoot their adult numbers. (B) Optimal lineage tree in which stem cells (red) first expand for three generations through symmetric divisions. In the fourth and final generation seven of the eight stem cells symmetrically divide into two nonstem cells (blue) and the remaining stem cell symmetrically divides into two stem cells, yielding the mature crypt in four generations. The resulting population dynamics are shown in (D). (C and E) The optimal solution if stem cell numbers are not allowed to overshoot ($q(t) \leq p(t)$) includes one generation in which a symmetric stem cell division generates the adult pool of two stem cells followed by a switch to asymmetric divisions generating the nonstem cells. Because nonstem cells exist longer than in (B) and (D) their overall extrusion is higher and the total time to a mature crypt in (C) and (E) exceeds that for the solution in (B) and (D). Note that the population dynamics in (E) will remain unchanged if in the second phase equal fractions of stem cells will symmetrically divide into either two stem cells or two nonstem cells ($p = q$), rather than having all dividing strictly asymmetrically. Nonstem cells are extruded with rate $\alpha = 0.3$.

under a fluorescence microscope. To facilitate the assignment of mRNA to individual cells we combined our transcript detection with immunofluorescence with the cell border marker E-cadherin (Figure S2C), as well as DAPI nuclear staining. In 5-day old mice crypt morphogenesis is at its peak and crypts of all sizes, ranging from a few cells per longitudinal section to the adult size of 30 cells per section can be observed (Figures 4B–4D), offering a comprehensive sampling

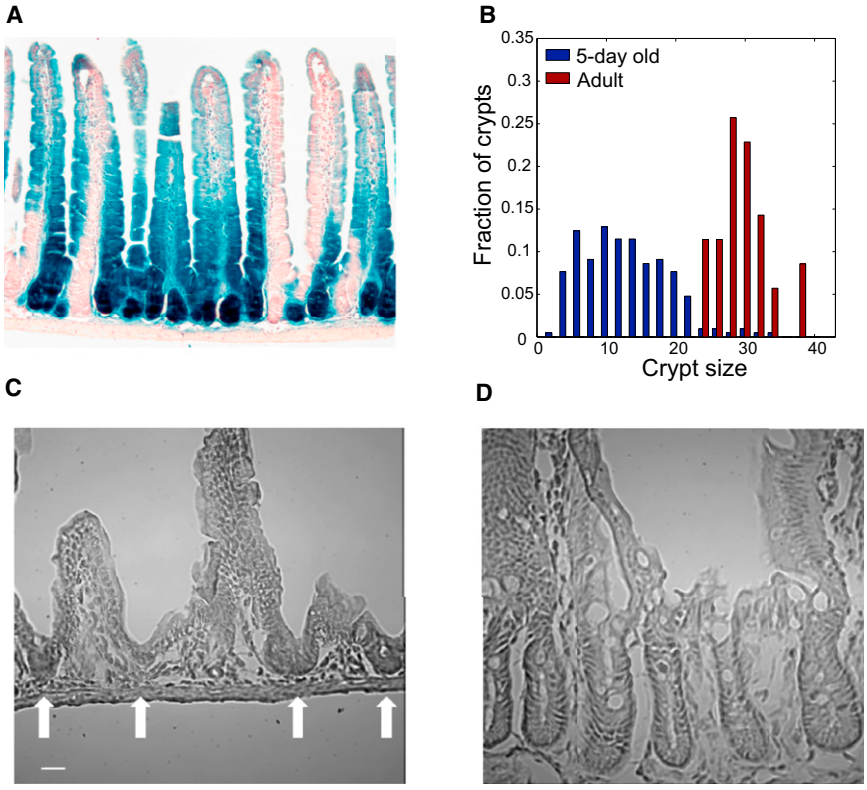

Figure 4. Lgr5 Marks Stem Cells in Developing Crypts

(A) Progenies of Lgr5 cells extend from the crypts through the villi. Duodenum from 5-day-old *Lgr5-EGFP-IRES-CreERT2/Rosa26*$^{LSL\text{-}lacZ}$ mouse injected with tamoxifen and sacrificed after 4 weeks. Blue cells are progenies of Lgr5 cells that express the lacZ reporter gene.

(B) Distributions of crypt sizes in 5-day-old mice (blue) and adult mice (red). Crypt size is the number of cells along an outline in a crypt longitudinal cross-section. Small intestine of 5-day-old mice contains crypts of variable sizes spanning the entire developmental process.

(C) H&E staining of duodenum from a 5-day-old mouse. Arrows mark crypts of variable sizes budding from the intervillus pockets.

(D) Duodenum from an adult mouse shows larger and more uniform sized crypts. Scale bars represent 20 μm (C and D). See also Figure S2.

of crypts at all stages of the morphogenetic process. To complement the dataset we also measured tissue from adult (4-month-old) mice (Figures 4B–4D). Thus, our experimental setup constitutes a sensitive and specific method to study stem cells within their anatomical context along the entire developmental process.

The Proliferation Rates of Stem Cells and Nonstem Cells Are at Their Maximal Level during Crypt Morphogenesis

Our theory predicts that mature crypts would be attained at the minimal time if both stem cells and nonstem cells divide at the fastest possible rate ($\beta_n = \beta_N = \beta_{max}$). The overall proliferation rates of crypt epithelial cells in infant mice has been shown to be the highest throughout life (Thrasher and Greulich, 1965), however, a comparative study of proliferation rates of stem cells and nonstem cells has not been conducted. To address this, we injected infant and adult mice with EdU, a modified nucleoside incorporated into DNA during S-phase, and sacrificed them after 60–90 min. We then performed single-molecule FISH for Lgr5, combined with fluorescent detection of EdU (Figure 5). Because the duration of S-phase is approximately constant for a broad range of cell types (Cameron and Greulich, 1963; Quastler and Sherman, 1959; Thrasher and Greulich, 1966) and invariant to mouse age (Thrasher and Greulich, 1965), proliferation rate directly correlates with the fraction of cells that are in S-phase (Quastler and Sherman, 1959) (Experimental Procedures).

We found that adult Lgr5+ cells have a cell cycle period of 22.4 ± 2.9 hr (Figure 5), in excellent agreement with previous estimates (Schepers et al., 2011). This period was significantly longer than the cell cycle period of Lgr5+ cells in crypts from infant mice (15.7 ± 1.8 hr). Importantly the cell cycle period of Lgr5+ cells in infant mice was not significantly different than that for Lgr5− cells in either infant (16.9 ± 1.7 hr) or adult mice (16.2 ± 1.7 hr). Thus proliferation rates of Lgr5 stem cells and of nonstem cells is identical in infant mice and is higher than in adult crypts, consistent with our model's predictions.

To further assess the proliferation status in developing crypts, we performed both single-molecule FISH and immunohistochemistry for Ki67 (Brizova et al., 2010) (Figure S3). Crypt cells exhibited uniform nuclear staining for Ki67 protein (Figure S3A). In addition, we found that the transcriptional levels of Ki67 were comparable between Lgr5+ and Lgr5− cells and were unchanged over a wide range of crypt sizes, again in agreement with our prediction that $\beta_n = \beta_N$ (Figures S3B and S3C). By analyzing the positions along the crypt axis of Lgr5 cells, we found that Lgr5 cells are confined to crypt bottoms in larger crypts and are not found on villi, consistent with our model assumption that they are not extruded (Figure S3D). Taken together these results indicate that the proliferation rates of stem cells and nonstem cells in developing crypts are identical and that only nonstem cells are extruded from the crypts. Therefore, $\beta_n > \beta_N - \alpha$. In this regime our optimal control theory predicts that a mature crypt would be attained in the shortest time if expansion of the entire stem cell pool would precede a transition to nonstem cell production (Figures 2D and 2F).

Stem Cell Dynamics Fit the Bang-Bang Control Solution

To test the temporal order predicted from the optimal bang-bang control solution we counted the number of Lgr5+ cells in duodenal crypts of different sizes, spanning all stages of the crypt morphogenetic process. We found that small crypts

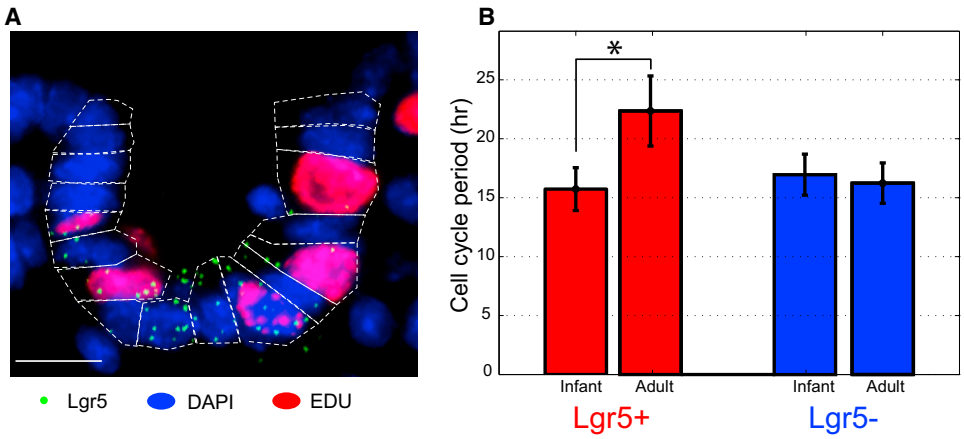

Figure 5. Lgr5+ Stem Cells and Lgr5− Cells Divide at the Fastest Possible Rate during Crypt Morphogenesis

(A) Combined detection of single Lgr5 mRNA (green dots) and EdU (red nuclei) in a small intestinal crypt from a 6-day-old mouse. Blue is DAPI nuclear staining and the dashed lines are cell borders. Scale bar represents 10 μm.

(B) The estimated cell cycle period in 6-day-old epithelial cells is about 15 hr for both Lgr5+ and Lgr5− cells in developing crypts. In adult crypts Lgr5+ cells proliferate more slowly (cell cycle time of 23 hr) whereas the Lgr5− cells divide once every 15 hr. Quantification was done only on cells that were positive for Ki67, detected using single-molecule FISH. Error bars represent standard errors of the mean across different crypts.

were almost entirely composed of Lgr5 positive cells (Figure 6). The number of these cells increased as crypts expanded, until it saturated at the number of Lgr5 cells seen in adults, 10 cells per longitudinal crypt section. Crypts larger than 10 cells per section continued to expand by adding Lgr5-negative cells while maintaining the saturation level of 10 stem cells (Figure 6B). The dynamics of stem cell numbers exhibited an excellent fit to the bang-bang control solution (Figures 6B and 6C). Importantly, the dynamics observed were dramatically different than that expected from a crypt with purely asymmetrically dividing stem cells (Figure 1A and Figure 6C, cyan curve) or from crypts maintaining constant stem cell fractions (Figure 1B and Figure 6C, red line). When examining stem cell numbers n versus crypt size C the bang-bang optimal control solution becomes independent of all rate parameters (β_n, β_N, α). It has a single defining hallmark: a linear increase in the number of stem cells versus crypt size ($n = C$) up to a crypt size that equals the size of the adult stem cell pool, and subsequent constant stem cell numbers (Figure 6B). We observed a similar behavior of stem cell dynamics in both the jejunum and ileum of the developing intestine (Figure S4).

Paneth Cells Appear after Stem Cell Numbers Saturate

It has recently been suggested that Paneth cells constitute the niche cells that supply the necessary signals to control the proliferation mode of Lgr5 stem cells in adult crypts (Sato et al., 2011). To assess whether the appearance of Paneth cells coincides with the transition that stem cells make to asymmetric divisions we measured the numbers of Paneth cells, as well as differentiated goblet cells per crypt using single-molecule FISH probe libraries for the markers Lysozyme and Gob5, respectively. Both Paneth and goblet cells appeared in larger crypts, at a later stage not congruent with the transition point (Figure 6B). Thus Paneth cells are not responsible for the switch in the stem cell proliferation mode during crypt morphogenesis.

Single-Cell Asymmetric Divisions during Crypt Morphogenesis

Our in situ measurements revealed a transition from a phase of purely symmetric divisions, in which the entire stem cell pool is established first, to a phase of asymmetric divisions, in which stem cells maintain their numbers while generating nonstem cells. We next asked whether the asymmetric phase consists of asymmetric divisions at the single stem cell level, or rather at the population level. Asymmetric divisions of each stem cell maintain stem cell numbers while generating new nonstem cells. Alternatively the asymmetric phase could consist of a population process in which a faction p of the stem cells divide symmetrically into two stem cells, whereas another fraction q divide symmetrically into two nonstem cells (Figure 3A). If these fractions are equal ($p = q$) stem cell numbers will again be maintained as new nonstem cells are generated. Crypt homeostasis in adult mice is dominated by population asymmetry (Lopez-Garcia et al., 2010; Snippert et al., 2010) ($p = q = 0.5$).

To study the modes of division of individual stem cells we performed short-term lineage tracing of progenies of Lgr5+ cells. We injected *Lgr5-EGFP-IRES-CreERT2*, *Rosa26*$^{LSL\text{-}tdTomato}$ infant mice with low doses of tamoxifen and sacrificed them after 1 day. We next assessed the Lgr5 status of pairs of labeled cell progenies. Population asymmetry would have given rise to pairs in which both cells are either Lgr5+ or Lgr5−. Single-cell asymmetric divisions should give rise to mixed pairs in which one progeny remains an Lgr5+ cell, whereas the other shuts down Lgr5 expression.

We found that small crypts were dominated by pairs of cells that were both Lgr5+ (89 ± 1%), consistent with the initial symmetric division phase. In contrast, larger crypts predominantly contained mixed pairs (75 ± 13%), with one Lgr5+ and one Lgr5− cell (Figure 7). Importantly, we detected no labeled pairs that were Lgr5−. This picture is consistent with asymmetric divisions at the single-stem cell level, and contrasts with the

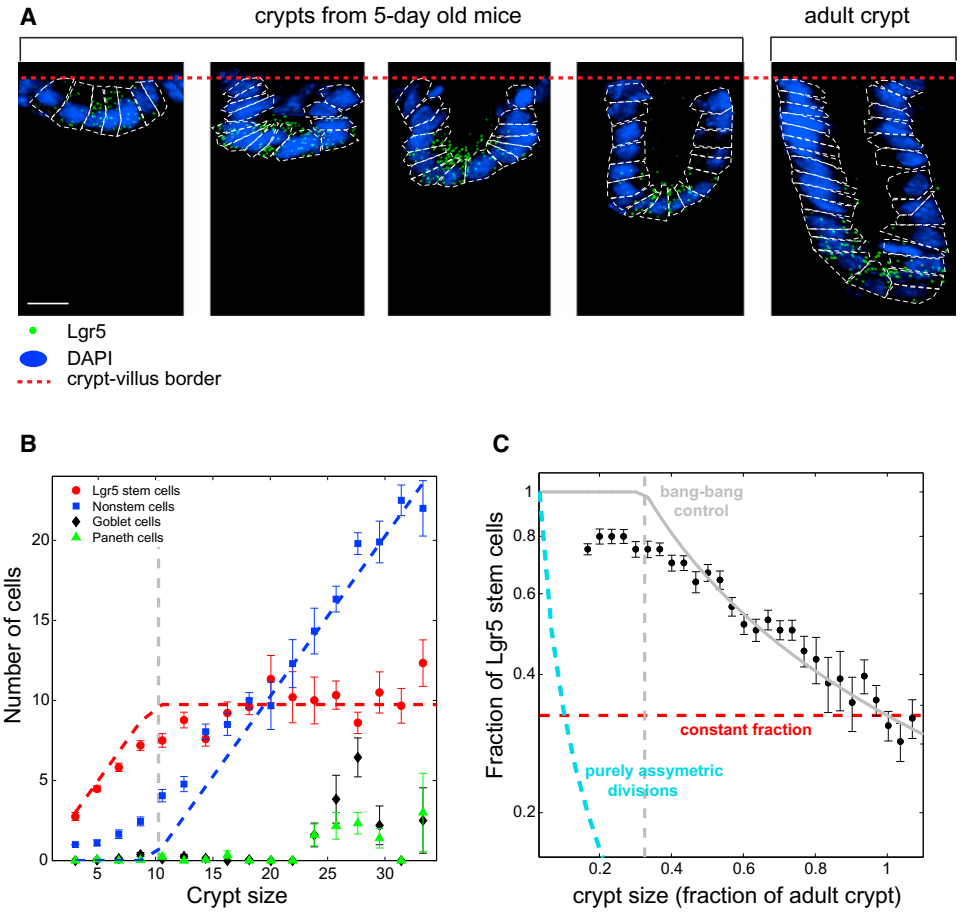

Figure 6. Stem Cell Dynamics in Developing Crypts Fit the Bang-Bang Control Solution

(A) Single-molecule FISH of Lgr5 in small intestinal frozen sections of 5-day-old mice and adult mice. Green dots are single Lgr5 transcripts, dashed lines denote the crypt cells. Blue is DAPI nuclear staining and the dashed red line denotes the crypt-villus border. Scale bar represents 10 μm. Cell segmentation was based on the DAPI image and simultaneous immunofluorescence with FITC labeled E-cadherin antibody (Figure S2C).

(B) Crypt dynamics displays a temporal order. Small crypts are exclusively composed of Lgr5 stem cells. When the crypt reaches a size equal to the number of Lgr5 stem cells in the adult crypt (10 cells per crypt longitudinal section, gray vertical dashed line) a transition to nonstem cell production occurs. Goblet cells (black diamonds) and Paneth cells (green triangles) appear at later developmental stages. Dashed red and blue curves are the dynamics predicted from the optimal control solution.

(C) Fraction of stem cells as a function of crypt size fits the bang-bang control solution (gray curve). Also shown are the expected dynamics under purely asymmetric stem cell divisions (cyan dashed curve) and constant fraction of stem cells and nonstem cells (red dashed line). Symbols and error bars in (B) and (C) are means and standard errors, respectively, of values in a moving window of five cells. This analysis was based on 248 crypts. See also Figure S4.

population asymmetry observed in adults (Lopez-Garcia et al., 2010; Snippert et al., 2010).

DISCUSSION

An important challenge in systems biology is to understand the design principles of stem cell-maintained tissues. Here we combined theoretical modeling, lineage tracing and sensitive in situ measurements to uncover a novel design principle—a temporal order that includes an initial expansion of the entire stem cell pool, followed by a transition to nonstem cell production. Our optimal control model demonstrated that such behavior, born of the choice that stem cells make between symmetric and asymmetric divisions, minimizes the time to achieve a mature crypt. The optimal solution is not sensitive to the initial number of stem cells per crypt, which is thought to be greater than one (Schmidt et al., 1988). It also remains valid when considering a fixed life span of nonstem cells as well as a wide range of temporally varying extrusion rates (Supplemental Information). Such variations in the extrusion rates could be a result of crypt growth, as well as to the simultaneous expansion of the villi, which we have not included in our model. As long as the extrusion rate is nonzero, the bang-bang control remains optimal for achieving a mature crypt as fast as possible.

When considering the possibility of symmetric divisions of a stem cell into two nonstem cells (Lopez-Garcia et al., 2010; Snippert et al., 2010), we found that a mature crypt could be obtained more rapidly if stem cell numbers overshoot their adult pool size (Figure 3). Similar dynamics, involving an overshoot in the number of progenitor cells followed by a complete loss as

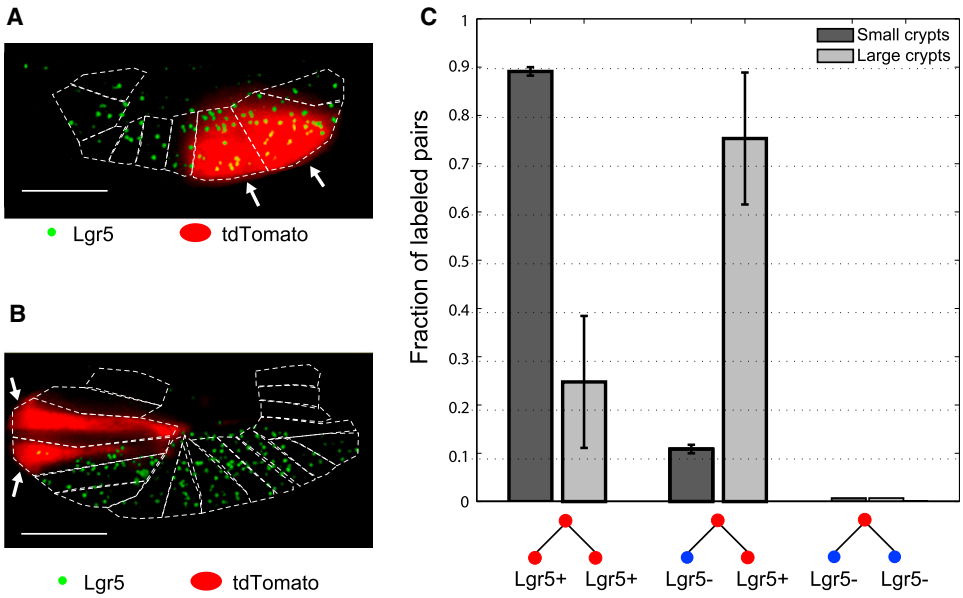

Figure 7. Asymmetric Phase during Crypt Morphogenesis Entails Asymmetric Divisions of Individual Stem Cells

(A) Example of a small crypt with a pair of Lgr5+ cells expressing the tdTomato reporter, representing the progenies of a symmetric division.

(B) Example of a larger crypt with a mixed pair in which one progeny is an Lgr5+ cell and the second progeny is Lgr5−. White arrows in (A) and (B) mark labeled cells. Scale bar represents 10 μm.

(C) Analysis of the Lgr5 status of labeled pairs of cells (with tdTomato fluorescence) in crypts with exactly two labeled cells. Small crypts (less than 12 cells per crypt outline) exhibit mostly pairs of cells that are both Lgr5+. Larger crypts contain mixed pairs, in which one progeny is Lgr5+ and the second is Lgr5−. No pair of labeled cells both lacking Lgr5 expression was found. Error bars represent standard error of the mean over two mice.

the differentiated progenies emerge, appears to be the strategy in the development of neocortical neurons (Nowakowski et al., 2002). It is interesting to hypothesize why this strategy is avoided in developing intestinal crypts. Unlike neuronal progenitors, crypt stem cells are not transient, but rather remain in the adult tissue. It could be that a solution entailing an overshoot is more sensitive to errors in the choice of proliferation modes (Lander et al., 2009). Excessive stem cell division into nonstem cells could lead to a complete loss of all the crypt stem cells.

Our short-term lineage tracing experiments revealed that the asymmetric phase in which nonstem cells are generated consists of asymmetric divisions of individual stem cells, which is distinct from the population asymmetry seen in adult crypts. This finding could be related to the absence of Paneth cells in the early crypt morphogenetic process. Paneth cells have been suggested to play an important role in coordinating the two different symmetric division modes of Lgr5+ cells in adults, which gives rise to the population asymmetry (Sato et al., 2011; Snippert et al., 2010). It will be interesting to further explore the transitions that crypts make from single-cell asymmetry to population asymmetry.

It is important to stress that other models can give rise to the stem cell dynamics we observed. For example, if stem cells have a protective role for the crypt, the initial formation of the stem cell compartment could enhance the probability of its survival. In addition, our model assumed that any stem cell proliferation strategy is feasible during the process. Different spatial or temporal constraints could limit the range of possible stem cell strategies.

The morphogenetic temporal order uncovered in our study could be a general design principle governing the development of other stem cell maintained tissues. Germ line stem cells in *C. elegans* symmetrically proliferate to increase their numbers during the early larval stages, while differentiated germ cells entering meiosis only appear at later stages (Kimble and Crittenden, 2007). A similar transition occurs in the embryonic development of the stratified mouse epidermis. At embryonic day 12.5, more than 90% of cell divisions are symmetric divisions that are parallel to the basal layer and that expand basal progenitors, whereas at embryonic day 14.5 most divisions are perpendicular, generating the more committed suprabasal progenitors (Lechler and Fuchs, 2005). In the mammalian neocortex, progenitor cells can divide symmetrically to increase their numbers, or differentiate to become postmitotic neurons. A majority of symmetric cell divisions that increase the number of progenitors precedes a transition to differentiation (Caviness et al., 1995; Nowakowski et al., 2002). In the mouse fetal liver hematopoietic stem cells exponentially proliferate between embryonic days 12 and 15, when their numbers saturate (Morrison et al., 1995a). It will be fascinating to apply similar approaches based on optimal control theory to explore the development, homeostasis and regeneration of these and other tissues.

EXPERIMENTAL PROCEDURES

Optimal Control Model

To solve the optimal control problem we minimized the time required to achieve a mature crypt, that is to transfer the system from the state (n_0,N_0)

to (n_T, N_T) subject to the constraints represented by Equations 1 and 2, and $0 \leq p(t) \leq 1$. Pontryagin's theorem states that the optimal control minimizes the Hamiltonian $H(t) = 1 + \lambda_1 dn/dt + \lambda_2 dN/dt$ where λ_1, λ_2 are Lagrange multipliers obeying specific costate equations (Supplemental Information). The Hamiltonian obtained by substituting Equations 1 and 2 is linear in the control function $p(t)$, and thus the minimum is obtained when $p(t)$ is set at one of its limits at each time point. The Supplemental Information provides a detailed analytical solution.

Mice and Tissues

Duodenum tissue was harvested from C57bl/6 female mice at ages 5 days (three mice), 6 days (two mice), and 4 months (two mice). *Lgr5-EGFP-IRES-CreERT2*, *Rosa26*$^{LSL\text{-}LacZ}$ *and Rosa26*$^{LSL\text{-}tdTomato}$ mice have been described previously (Barker et al., 2007; Madisen et al., 2010). Mice were euthanized by CO_2 asphyxiation. The tissue was removed, fixed immediately in 4% formaldehyde, then incubated overnight with 30% sucrose in 4% formaldehyde and then embedded in OCT. Cryosections (6 μm) were used for hybridizations. The MIT Institutional Animal Care and Use Committee approved all animal studies and procedures.

Single-Molecule FISH

Probe library construction and hybridization procedures were previously described in Itzkovitz et al. (2011). To detect cell borders we combined immunofluorescence with FITC conjugated E-cadherin antibody (BD Biosciences). DAPI dye for nuclear staining was added during the washes. For the EdU incorporation assay mice were injected with 100 μl (for 6-day-old mice) or 300 μl (adult mice) 3 mM EdU and sacrificed after 60–90 min. Click-iT staining (Click-iT EdU, Invitrogen) was performed after the RNA FISH hybridization washes. All images were taken with a Nikon Ti-E inverted fluorescence microscope equipped with a 100× oil-immersion objective and a Photometrics Pixis 1024 CCD camera using MetaMorph software (Molecular Devices, Downington, PA). The image-plane pixel dimension was 0.13 μm. Quantification was done on six optical sections with a z-spacing of 0.3 μm.

Data Analysis

Dots were automatically detected as described in Itzkovitz et al. (2011). The dot stack images were first filtered with a three-dimensional Laplacian of Gaussian filter of size 15 pixels and standard deviation of 1.5 pixels. The number of connected components in binary thresholded images was then recorded for a uniform range of intensity thresholds and the threshold for which the number of components was least sensitive to threshold selection was used for dot detection. Cell segmentation was manually performed based on the E-cadherin and DAPI stains. All cells within a crypt outline were segmented. The crypt-villus border was set at the cell position where an angle formed, as described in Bjerknes and Cheng (1981). The smallest crypt size analyzed had three cells per longitudinal section as the crypt-villus border could not be discerned for smaller crypts. Transcript concentrations were obtained by dividing the number of transcripts per cell by the cell volume estimated as the product of the segmented area and the number of vertical optical sections times a voxel size of 0.13 μm × 0.13 μm × 0.3 μm. Crypt apex and outline were manually marked and used to determine cell position along the crypt axis. Only cells that were strictly within the crypt borders were counted. These are expected to be progenies of the dividing crypt stem cells. This is especially important when counting goblet cells, as the intestinal villi of newborn mice abound with goblet cells that exist before initial crypt budding. Cell cycle period T_c was calculated based on the formula introduced by Quastler and Sherman (1959) $T_c = T_S/f$, where T_S is the S-phase time and f is the fraction of EdU positive cells. T_S was estimated at 7.5 hr (Cameron and Greulich, 1963; Quastler and Sherman, 1959; Thrasher and Greulich, 1966). To ensure exclusion of differentiated cells in the calculation of cell cycle period we cohybridized the samples for EdU with single-molecule FISH libraries for Ki67 and included only cells that were positive for Ki67 in the calculations.

Lineage Tracing Experiments

For long-term lineage tracing experiments we injected 0.4 mg tamoxifen into 5-day old *Lgr5-EGFP-IRES-CreERT2* C57Bl6/J mice bred to Rosa26$^{LSL\text{-}LacZ}$ reporter mice. Detection of lacZ was performed as previously described in Barker et al. (2007) (Figure 4A) and using single-molecule FISH (Figure S2A). The short-term lineage tracing results were based on two *Lgr5-EGFP-IRES-CreERT2*, *Rosa26*$^{LSL\text{-}tdTomato}$ mice, a P10 mouse injected with 1 μg tamoxifen and sacrificed after 24 hr, and a P11 injected with 10 μg and sacrificed after 16 hr. The P11 mouse also contained a floxed allele of Nkx2.1, which is not expressed in intestinal crypts (we validated this using single-molecule FISH, data not shown). Labeling was detected in less than 1/50 of crypt sections in the P10 mouse. The P11 mouse showed higher and more variable recombination rates, and we thus focused on duodenal regions with rare recombination events. We performed the analysis only on crypt sections that had exactly two tdTomato-labeled cells.

SUPPLEMENTAL INFORMATION

Supplemental Information includes Extended Experimental Procedures and four figures and can be found with this article online at doi:10.1016/j.cell.2011.12.025.

ACKNOWLEDGMENTS

We thank Uri Alon for suggesting the optimality problem. We thank Johan van Es for help with the lineage tracing experiments. We also thank George Oster, Hyun Youk, Stefan Semrau and Sandy Klemm for valuable discussions. This work was supported by the NIH/NCI Physical Sciences Oncology Center at MIT (U54CA143874) and a NIH Pioneer award (1DP1OD003936) to A.v.O. and in part by Cancer Center Support (core) grant P30-CA14051 from the National Cancer Institute. T.J. is a Howard Hughes Investigator and a Daniel K. Ludwig Scholar. S.I. acknowledges support from the International Human Frontiers Science Program Organization and the Machiah Foundation. I.B. acknowledges support from the Howard Hughes Medical Institute Gilliam fellowship.

Received: May 11, 2011
Revised: September 26, 2011
Accepted: December 20, 2011
Published: February 2, 2012

REFERENCES

Al-Nafussi, A.I., and Wright, N.A. (1982). Cell kinetics in the mouse small intestine during immediate postnatal life. Virchows Arch. B Cell Pathol. Incl. Mol. Pathol. *40*, 51–62.

Alon, U. (2006). An Introduction to Systems Biology: Design Principles of Biological Circuits (Chapman and Hall/CRC).

Barker, N., van Es, J.H., Kuipers, J., Kujala, P., van den Born, M., Cozijnsen, M., Haegebarth, A., Korving, J., Begthel, H., Peters, P.J., and Clevers, H. (2007). Identification of stem cells in small intestine and colon by marker gene Lgr5. Nature *449*, 1003–1007.

Bjerknes, M., and Cheng, H. (1981). The stem-cell zone of the small intestinal epithelium. II. Evidence from Paneth cells in the newborn mouse. Am. J. Anat. *160*, 65–75.

Blanpain, C., and Fuchs, E. (2006). Epidermal stem cells of the skin. Annu. Rev. Cell Dev. Biol. *22*, 339–373.

Brizova, H., Kalinova, M., Krskova, L., Mrhalova, M., and Kodet, R. (2010). A novel quantitative PCR of proliferation markers (Ki-67, topoisomerase IIalpha, and TPX2): an immunohistochemical correlation, testing, and optimizing for mantle cell lymphoma. Virchows Arch. *456*, 671–679.

Buske, P., Galle, J., Barker, N., Aust, G., Clevers, H., and Loeffler, M. (2011). A comprehensive model of the spatio-temporal stem cell and tissue organisation in the intestinal crypt. PLoS Comput. Biol. *7*, e1001045.

Cameron, I.L., and Greulich, R.C. (1963). Evidence for an essentially constant duration of DNA synthesis in renewing epithelia of the adult mouse. J. Cell Biol. *18*, 31–40.

Caviness, V.S., Jr., Takahashi, T., and Nowakowski, R.S. (1995). Numbers, time and neocortical neuronogenesis: a general developmental and evolutionary model. Trends Neurosci. *18*, 379–383.

Clayton, E., Doupé, D.P., Klein, A.M., Winton, D.J., Simons, B.D., and Jones, P.H. (2007). A single type of progenitor cell maintains normal epidermis. Nature *446*, 185–189.

Frank, S.A., Iwasa, Y., and Nowak, M.A. (2003). Patterns of cell division and the risk of cancer. Genetics *163*, 1527–1532.

Grey, R.D. (1968). Epithelial cell migration in the intestine of the young mouse. Dev. Biol. *18*, 501–504.

Itzkovitz, S., Lyubimova, A., Blat, I.C., Maynard, M., van Es, J., Lees, J., Jacks, T., Clevers, H., and van Oudenaarden, A. (2011). Single-molecule transcript counting of stem-cell markers in the mouse intestine. Nat. Cell Biol. *14*, 106–114.

Kimble, J., and Crittenden, S.L. (2007). Controls of germline stem cells, entry into meiosis, and the sperm/oocyte decision in Caenorhabditis elegans. Annu. Rev. Cell Dev. Biol. *23*, 405–433.

Kirk, D. (2004). Optimal Control Theory: An Introduction (Dover).

Klein, A.M., Nakagawa, T., Ichikawa, R., Yoshida, S., and Simons, B.D. (2010). Mouse germ line stem cells undergo rapid and stochastic turnover. Cell Stem Cell *7*, 214–224.

Komarova, N.L., Sadovsky, A.V., and Wan, F.Y. (2008). Selective pressures for and against genetic instability in cancer: a time-dependent problem. J. R. Soc. Interface *5*, 105–121.

Koo, D. (1977). Elements of Optimization: With Applications in Economics and Business (Springer).

Lander, A.D., Gokoffski, K.K., Wan, F.Y., Nie, Q., and Calof, A.L. (2009). Cell lineages and the logic of proliferative control. PLoS Biol. *7*, e15.

Lechler, T., and Fuchs, E. (2005). Asymmetric cell divisions promote stratification and differentiation of mammalian skin. Nature *437*, 275–280.

Lopez-Garcia, C., Klein, A.M., Simons, B.D., and Winton, D.J. (2010). Intestinal stem cell replacement follows a pattern of neutral drift. Science *330*, 822–825.

Macevicz, S., and Oster, G. (1976). Modeling social insect populations II: optimal reproductive strategies in annual eusocial insect colonies. Behav. Ecol. Sociobiol. *1*, 265–282.

Madisen, L., Zwingman, T.A., Sunkin, S.M., Oh, S.W., Zariwala, H.A., Gu, H., Ng, L.L., Palmiter, R.D., Hawrylycz, M.J., Jones, A.R., et al. (2010). A robust and high-throughput Cre reporting and characterization system for the whole mouse brain. Nat. Neurosci. *13*, 133–140.

Michor, F., Frank, S.A., May, R.M., Iwasa, Y., and Nowak, M.A. (2003). Somatic selection for and against cancer. J. Theor. Biol. *225*, 377–382.

Moore, K.A., and Lemischka, I.R. (2006). Stem cells and their niches. Science *311*, 1880–1885.

Morrison, S.J., Hemmati, H.D., Wandycz, A.M., and Weissman, I.L. (1995a). The purification and characterization of fetal liver hematopoietic stem cells. Proc. Natl. Acad. Sci. USA *92*, 10302–10306.

Morrison, S.J., and Kimble, J. (2006). Asymmetric and symmetric stem-cell divisions in development and cancer. Nature *441*, 1068–1074.

Morrison, S.J., Uchida, N., and Weissman, I.L. (1995b). The biology of hematopoietic stem cells. Annu. Rev. Cell Dev. Biol. *11*, 35–71.

Nowakowski, R.S., Caviness, V.S., Jr., Takahashi, T., and Hayes, N.L. (2002). Population dynamics during cell proliferation and neuronogenesis in the developing murine neocortex. Results Probl. Cell Differ. *39*, 1–25.

Perelson, A.S., Mirmirani, M., and Oster, G.F. (1976). Optimal strategies in immunology. I. B-cell differentiation and proliferation. J. Math. Biol. *3*, 325–367.

Potten, C.S., and Loeffler, M. (1990). Stem cells: attributes, cycles, spirals, pitfalls and uncertainties. Lessons for and from the crypt. Development *110*, 1001–1020.

Quastler, H., and Sherman, F.G. (1959). Cell population kinetics in the intestinal epithelium of the mouse. Exp. Cell Res. *17*, 420–438.

Raj, A., Rifkin, S.A., Andersen, E., and van Oudenaarden, A. (2010). Variability in gene expression underlies incomplete penetrance. Nature *463*, 913–918.

Raj, A., van den Bogaard, P., Rifkin, S.A., van Oudenaarden, A., and Tyagi, S. (2008). Imaging individual mRNA molecules using multiple singly labeled probes. Nat. Methods *5*, 877–879.

Reeves, G.T., and Fraser, S.E. (2009). Biological systems from an engineer's point of view. PLoS Biol. *7*, e21.

Sato, T., van Es, J.H., Snippert, H.J., Stange, D.E., Vries, R.G., van den Born, M., Barker, N., Shroyer, N.F., van de Wetering, M., and Clevers, H. (2011). Paneth cells constitute the niche for Lgr5 stem cells in intestinal crypts. Nature *469*, 415–418.

Schepers, A.G., Vries, R., van den Born, M., van de Wetering, M., and Clevers, H. (2011). Lgr5 intestinal stem cells have high telomerase activity and randomly segregate their chromosomes. EMBO J. *30*, 1104–1109.

Schmidt, G.H., Winton, D.J., and Ponder, B.A. (1988). Development of the pattern of cell renewal in the crypt-villus unit of chimaeric mouse small intestine. Development *103*, 785–790.

Slack, J.M. (2000). Stem cells in epithelial tissues. Science *287*, 1431–1433.

Snippert, H.J., van der Flier, L.G., Sato, T., van Es, J.H., van den Born, M., Kroon-Veenboer, C., Barker, N., Klein, A.M., van Rheenen, J., Simons, B.D., and Clevers, H. (2010). Intestinal crypt homeostasis results from neutral competition between symmetrically dividing Lgr5 stem cells. Cell *143*, 134–144.

Thrasher, J.D., and Greulich, R.C. (1965). The duodenal progenitor population. I. Age related increase in the duration of the cryptal progenitor cycle. J. Exp. Zool. *159*, 39–46.

Thrasher, J.D., and Greulich, R.C. (1966). The duodenal progenitor population. 3. The progenitor cell cycle of principal, goblet and Paneth cells. J. Exp. Zool. *161*, 9–19.

van der Flier, L.G., and Clevers, H. (2009). Stem cells, self-renewal, and differentiation in the intestinal epithelium. Annu. Rev. Physiol. *71*, 241–260.

Watt, F.M., and Hogan, B.L. (2000). Out of Eden: stem cells and their niches. Science *287*, 1427–1430.

Yatabe, Y., Tavaré, S., and Shibata, D. (2001). Investigating stem cells in human colon by using methylation patterns. Proc. Natl. Acad. Sci. USA *98*, 10839–10844.

EXTENDED EXPERIMENTAL PROCEDURES

Analytical Solution to the Optimal Control Model

In this section we formulate our optimal control model for crypt development and present its analytical solution. Our model considers two cell populations that differ in their proliferative dynamics – *n(t)* stem cells and *N(t)* nonstem cells (Figure 2). Stem cells divide with rate β_n and remain within the crypt indefinitely. Nonstem cells divide with rate β_N and are extruded from the crypt at rate α. Stem cells can divide either symmetrically into two stem cells with probability *p(t)* or asymmetrically into one stem cell and one nonstem cell with probability *1-p(t)*. The optimization goal is to transfer the initial state (n_0,N_0) to a final crypt size of (n_T,N_T) in the minimal time. We assume $n_T > n_0$, $N_T > N_0 = 0$, assumptions that are based on our experimental measurements (Figure 6).

The dynamics of the crypt populations is described by the state equations:

$$\frac{dn(t')}{dt'} = p(t')\beta_n n(t') \tag{1}$$

$$\frac{dN(t')}{dt'} = (1 - p(t'))\beta_n n(t') + (\beta_N - \alpha)N(t') \tag{2}$$

where t′ denotes time in non-scaled units and where $0 \leq p(t') \leq 1$. By using the rescaled time $t = \beta_n t'$ the equations become:

$$\frac{dn(t)}{dt} = p(t)n(t) \tag{1}$$

$$\frac{dN(t)}{dt} = (1 - p(t))n(t) + bN(t) \tag{2}$$

where $b = (\beta_N - \alpha)/\beta_n$

The optimization goal is to minimize the time, *T* to obtain a mature crypt:

$$T = \int_0^T 1\, dt \tag{3}$$

Subject to the constraints in Equations (1, 2), $0 \leq p(t) \leq 1$ and with the boundary conditions: $n(0) = n_0$, $N(0) = 0$, $n(T) = n_T > n_0$, $N(T) = N_T > 0$. Following Kirk (Kirk, 2004) we introduce Lagrange multipliers λ_1, λ_2 for constraints (1) and (2) to form the Hamiltonian:

$$H(t) = 1 + \lambda_1 pn + \lambda_2(1 - p)n + \lambda_2 bN = (\lambda_1 - \lambda_2)np + 1 + \lambda_2(n + bN) \tag{4}$$

Pontryagin's minimum theory states that a necessary condition for a control function *p(t)* to minimize the total time *T* is that it minimizes the Hamiltonian of Equation (4) at each time point. Additionally, since the final time *T* is free and the Hamiltonian does not explicitly depend on time, the Hamiltonian is identically zero at the extremal trajectory (Kirk, 2004):

$$H(t) = 0 \tag{5}$$

Equation (4) indicates that the Hamiltonian is a linear function of *p(t)* at any time point *t*. It will thus be minimized by setting *p* at either its minimal or maximal allowed value, depending on whether the slope in Equation (4), $(\lambda_1 - \lambda_2)n$ is positive or negative respectively. This solution is termed a 'bang-bang' control (Kirk, 2004; Macevicz and Oster, 1976; Perelson et al., 1976). Since *n(t) > 0*, the solution will depend on the sign of the switching function $\sigma(t) = \lambda_1(t) - \lambda_2(t)$:

$$p(t) = \begin{cases} 0 & \lambda_1(t) - \lambda_2(t) > 0 \\ 1 & \lambda_1(t) - \lambda_2(t) < 0 \end{cases} \tag{6}$$

This solution indicates that at any given time all stem cells should employ the same proliferation mode – either all stem cells divide symmetrically (*p(t) = 1*) or all stem cells divide asymmetrically (*p(t) = 0*). We will next show that the control function switches only once during the process, and will determine the switching time, as well as the total time *T* for the optimal solution. The Lagrange multipliers obey the following co-state equations (Kirk, 2004):

$$\frac{d\lambda_1(t)}{dt} = -\frac{\delta H}{dn} = -\lambda_2 + (\lambda_2 - \lambda_1)p \tag{7}$$

$$\frac{d\lambda_2(t)}{dt} = -\frac{\delta H}{dN} = -b\lambda_2 \tag{8}$$

Equation (8) does not depend on *p(t)* and its solution is:

$$\lambda_2(t) = \lambda_2(T)e^{-b(t-T)} \tag{9}$$

To solve $\lambda_1(t)$ We will next consider the two possible cases at *T*, *p(T) = 1* and *p(T) = 0*:

Case 1

p(T) = 1 (and $\lambda_1(T) < \lambda_2(T)$ from Equation (6)). From Equations (4, 5):

$$H(T) = 1 + \lambda_1(T)n_T + \lambda_2(T)bN_T = 0 \tag{10}$$

And thus:

$$\lambda_1(T) = -\frac{1 + \lambda_2(T)bN_T}{n_T} < \lambda_2(T) \tag{11}$$

We next set *p(T) = 1* in Equation (7) to solve for $\lambda_1(t)$ at times approaching T:

$$\lambda_1(t) = \lambda_1(T)e^{-(t-T)} \tag{12}$$

Since *p(T)* = 1, the solution *p(t)* will only be possible if there is a switch, that is $0 < \tau < T$ for which $\lambda_1(\tau) = \lambda_2(\tau)$. This is because *N(0) = 0* and Equation (2) shows that *N(t)* can only increase if *p(t) < 1* for a part of the process. From Equations (9, 11, 12) this will only be possible if $\lambda_2(T) \leq 0$. Additionally, since $\lambda_1(T) < \lambda_2(T)$ we must have *b > 1*, or else $\lambda_1(t) < \lambda_2(t)$ and *p(t) = 1* for all $0 < t < T$. Thus a reachable extremal solution for which *p(T) = 1* is possible only if *b > 1*. We will next calculate the switching time and show that there is only one switch. At the transition point:

$$\lambda_1(\tau) = \lambda_1(T)e^{-(\tau-T)} = \lambda_2(T)e^{-b(\tau-T)} = \lambda_2(\tau) \tag{13}$$

The solution of Equation (13) is:

$$\tau = T + \frac{1}{b-1}\ln\left(\frac{\lambda_2(T)}{\lambda_1(T)}\right) = T + \frac{1}{b-1}\ln\left(-\frac{n_T\lambda_2(T)}{1 + bN_T\lambda_2(T)}\right) \tag{14}$$

where we have used Equation (11). Prior to the switch, at $t < \tau$, *p(t) = 0*. Using Equation (7) we find:

$$\lambda_1(t) = \lambda_1(\tau) + \frac{\lambda_2(T)}{b}\left[e^{-b(t-T)} - e^{-b(\tau-T)}\right] \tag{15}$$

Equation (15) indicates that $\lambda_1(t) > \lambda_2(t)$ for all $0 < t < \tau$, and thus the switch at τ is the only transition during the process. This solution can be intuitively understood by noting that if $b>1$, $\beta_N - \alpha > \beta_n$, and the nonstem cell yield per nonstem cell is higher than that for a stem cell. It is thus more productive to generate as many nonstem cells first and then switch to producing stem cells, as existing nonstem cells would propagate their numbers faster than the flux obtained from existing stem cells. To summarize, the solution for which *p(T) = 1* is:

$$p = \begin{cases} 0 & 0<t<\tau \\ 1 & \tau<t<T \end{cases} \tag{16}$$

And requires *b > 1*.

We will next use Equations (1, 2, 16) to solve for the switching time τ and the final time *T* in terms of (n_0,N_0, n_T,N_T). Solving Equation (1) for $t > \tau$:

$$n(t) = n_0 e^{t-\tau} \tag{17}$$

And using $n(T) = n_T$:

$$T - \tau = \ln\left(\frac{n_T}{n_0}\right) \tag{18}$$

Solving Equation (2) for $0 < t < \tau$, and using *N(0) = 0*:

$$N(t) = \frac{n_0}{b}\left(e^{bt} - 1\right) \tag{19}$$

And at $t > \tau$:

$$N(t) = N(\tau)e^{b(t-\tau)} = \frac{n_0}{b}\left(e^{b\tau} - 1\right)e^{b(t-\tau)} \tag{20}$$

Setting $N(T) = N_T$ in Equation (20) and using Equation (18):

$$\tau = \frac{1}{b}\ln\left(1 + \frac{bN_T}{n_0}\left(\frac{n_0}{n_T}\right)^b\right) \tag{21}$$

Finally using Equation (18):

$$T = \ln\left(\frac{n_T}{n_0}\right) + \frac{1}{b}\ln\left(1 + \frac{bN_T}{n_0}\left(\frac{n_0}{n_T}\right)^b\right) \tag{22}$$

Equations (21, 22) provide us with the switching time and the total time.

Case 2

We now consider the second possibility consistent with the bang-bang control, $p(T) = 0$, or using (6), $\lambda_1(T) > \lambda_2(T)$. From Equations (4, 5):

$$\lambda_2(T) = -\frac{1}{n_T + bN_T} \tag{23}$$

Equation (9) still describes the temporal dynamics of $\lambda_2(t)$ for $0 < t < T$, as this is independent of $p(t)$. To solve the dynamics of $\lambda_1(t)$ at times approaching T we set $p(t) = 0$ in Equation (7):

$$\lambda_1(t) = \lambda_1(T) - \lambda_2(T)\frac{1 - e^{-b(t-T)}}{b} = \lambda_1(T) + \frac{1 - e^{-b(t-T)}}{b(n_T + bN_T)} \tag{24}$$

And the switching function is:

$$\sigma(t) = \lambda_1(t) - \lambda_2(t) = \lambda_1(T) - \lambda_2(T)\left(\frac{1}{b} + \left(1 - \frac{1}{b}\right)e^{-b(t-T)}\right) \tag{25}$$

Since $\sigma(T) > 0$ (from Equation (6)) the solution will be feasible only if a switch $\sigma(\tau) = 0$ occurs at some time $0 < \tau < T$. This is because $n_T > n_0$ and an increase in stem cell number cannot occur if $p(t) = 0$ for all $0 < t < T$. Thus from Equation (25) $\sigma(t)$ will cross zero only if $b < 1$. By setting $\sigma(\tau) = 0$ we find the switching time:

$$\tau = T - \frac{1}{b}\log\left(\frac{b}{b-1}\right) - \frac{1}{b}\log\left(\frac{\lambda_1(T)}{\lambda_2(T)} - \frac{1}{b}\right) \tag{26}$$

At times prior to the switch ($0 < t < \tau$) we use $p(t) = 1$ in Equation (7) to solve for the switching function:

$$\sigma(t) = \lambda_1(\tau)e^{t-\tau} - \lambda_2(\tau)e^{b(t-\tau)} < 0 \tag{27}$$

Where we used $\lambda_1(\tau) = \lambda_2(\tau)$ and the fact that $b < 1$. Thus a switch occurs only once. To summarize case 2, if $b < 1$ the optimal solution is:

$$p = \begin{cases} 1 & 0 < t < \tau \\ 0 & \tau < t < T \end{cases} \tag{28}$$

Solving Equation (1) using Equation (28):

$$n(t) = n_0 e^t \tag{29}$$

And using $n(\tau) = n_T$:

$$\tau = \ln\left(\frac{n_T}{n_0}\right) \tag{30}$$

Solving Equation (2) for $\tau < t < T$ and using $N(\tau) = 0$:

$$N(t) = \frac{n_T}{b}\left(e^{b(t-\tau)} - 1\right) \tag{31}$$

And using $N(T) = N_T$:

$$T = \ln\left(\frac{n_T}{n_0}\right) + \frac{1}{b}\ln\left(1 + \frac{bN_T}{n_T}\right) \tag{32}$$

Note that Equations (32) and (22) converge as b approaches 1.

Singular Intervals

Equation (6) indicates that the control function (stem cell symmetric division probability, $p(t)$) will always assume either its upper or lower limit, depending on whether the switching function $\sigma(t) = \lambda_1(t) - \lambda_2(t)$ is negative or positive respectively. The control function switches between its limit values at times when the switching function is zero. Singular intervals occur if $\sigma(t) = 0$ over a non-zero time interval. For this to occur, all the temporal derivatives of $\sigma(t)$ should be identically zero over this interval. Thus in a singular interval we would have:

$$\sigma(t) = \lambda_1(t) - \lambda_2(t) = 0 \Rightarrow \lambda_1(t) = \lambda_2(t) \tag{33}$$

$$\frac{d\sigma(t)}{dt} = \frac{d\lambda_1(t)}{dt} - \frac{d\lambda_2(t)}{dt} = -\lambda_2 + (\lambda_2 - \lambda_1)p + b\lambda_2 = 0 \Rightarrow b = 1 \tag{34}$$

Where we used the co-state Equations (7, 8) in Equation (34). Thus in the specific case when $b = 1$ the control function cannot be determined over the entire developmental process. Indeed, this case implies that the nonstem cell yield per dividing nonstem cell ($\beta_N - \alpha$) is equal to that from a dividing stem cell (β_n), and thus all feasible stem cell division strategies (functions $p(t)$ that are able to transfer the system from the initial state (n_0, N_0) to the final state (n_T, N_T)) will take the same time.

To summarize, the optimal solution for achieving a mature crypt in minimal time is:

$$\begin{array}{llll}
\boldsymbol{\beta_n < \beta_N - \alpha} & & & \\
0 \le t \le \tau & p(t) = 0 & n(t) = n_0 & N(t) = \frac{n_0}{b}\left(e^{bt} - 1\right) \\
\tau \le t \le T & p(t) = 1 & n(t) = n_0 e^{t-\tau} & N(t) = \frac{n_0}{b}\left(e^{b\tau} - 1\right)e^{b(t-\tau)} \\
\boldsymbol{\beta_n > \beta_N - \alpha} & & & \\
0 \le t \le \tau & p(t) = 1 & n(t) = n_0 e^{t} & N(t) = 0 \\
\tau \le t \le T & p(t) = 0 & n(t) = n_T & N(t) = \frac{n_T}{b}\left(e^{b(t-\tau)} - 1\right)
\end{array}$$

Bang-Bang Control Remains the Optimal Solution When Considering Fixed Life Span of Nonstem Cells

Our optimization model assumed that the rate at which a nonstem cell is extruded from the crypt is uniform and independent of its 'birth' time - the time when it first divided from a stem cell. Intestinal cells migrate along the crypt axis as they divide, and a more realistic representation could consider extrusion rates that depend on the number of divisions that nonstem cell have undergone since their birth. Thus rather than having an exponentially decaying life time with rate α the life span of a nonstem cell would be a step function – cells will divide for precisely u generations and at generation u will be extruded. To study this possibility we performed lineage simulations of this process and numerically searched for the optimal stem cell probability function using a combinatorial optimization algorithm.

For simplicity we considered synchronous divisions of all cells with equal rates for stem cells and nonstem cells ($\beta_n = \beta_N$). For each probability function $p(t)$, where $t = 1,2,\ldots$ are discrete generation times, we simulated 100 different trees in which non stem cells divided for exactly u generations before being extruded. All trees were initiated with one stem cell and required to reach a final preset number of stem cells and nonstem cells. We scored each resulting lineage tree by the minimal time required to obtain the final state (to accelerate the simulations we allowed final nonstem cell counts that were within the range of 5 cells from the required final number). Trees in which the required size was not attainable received a penalty score that is 2 generations higher than the minimal possible time. Each probability function was assigned an average score S_i in 100 iterations.

At each stage i we performed a random change in the probability function $p_i(t)$ and retested a new function $p_j(t)$. $p_j(t)$ was obtained by always changing the symmetric division probability at random at one randomly chosen time point, changing at random at a second time point with probability 50% and at a third time point with probability 10% (these rules were heuristically chosen to accelerate the search of the space of possible probability functions). The scoring function for the new probability, S_j, was recalculated and a simulated annealing decision rule was employed – the new function $p_j(t)$ was accepted either if $S_j < S_i$ or at random with probability $e^{-\Delta S/\eta}$, where $\Delta S = S_j - S_i$ (note that we favor lower scores or average times to a mature crypt). η serves as a 'temperature' which allows the search to avoid being stuck in local minima. Our simulations started with temperature $T = 0.5$ and lowered it by 4% every 100 steps

(Monte Carlo sweeps). Each simulation was initiated several times with different initial probability functions and was run until convergence. The search converged on the 'bang-bang' control each time (Figure S1).

Bang-Bang Control Remains the Optimal Solution When Considering Variable Extrusion Rates

Our optimization model assumed a constant extrusion rate throughout the crypt developmental process. However, this rate could potentially vary due to both crypt growth and to the simultaneous expansion of the villi. For example, if nonstem cells are migrating at a constant speed throughout the process, the rate at which they exit the crypts would increase as crypts enlarge. To explore these effects we performed numerical simulations of the developmental process and searched for the optimal proliferation strategy under a wide range of variable extrusion rates.

As in the simulations of fixed extrusion rates we performed Monte Carlo simulations where for simplicity we considered synchronous divisions of all cells with equal rates for stem cells and nonstem cells ($\beta_n = \beta_N$). Different proliferative probability functions $p(t)$ were iteratively tested for the time to obtain a mature crypt and accepted according to the same simulated annealing rule used in the fixed-life-span simulations. In the present simulations, however, we eliminated cells with a temporally-varying extrusion rate $\alpha(t)$. We tested a wide range of $\alpha(t)$, including monotonously increasing or decreasing functions between $0.05\beta_n$ and $0.8\beta_n$, as well as randomly fluctuating extrusion rates with a coefficient of variation ranging from 0.1 to 0.6. The bang-bang control solution achieved the mature crypt at the minimal time for all variable extrusion rates tested.

SUPPLEMENTAL REFERENCES

Kirk, D. (2004). Optimal Control Theory: An Introduction (Dover).

Macevicz, S., and Oster, G. (1976). Modeling social insect populations II: Optimal reproductive strategies in annual eusocial insect colonies. Behav. Ecol. Sociobiol. *1*, 265–282.

Perelson, A.S., Mirmirani, M., and Oster, G.F. (1976). Optimal strategies in immunology. I. B-cell differentiation and proliferation. J. Math. Biol. *3*, 325–367.

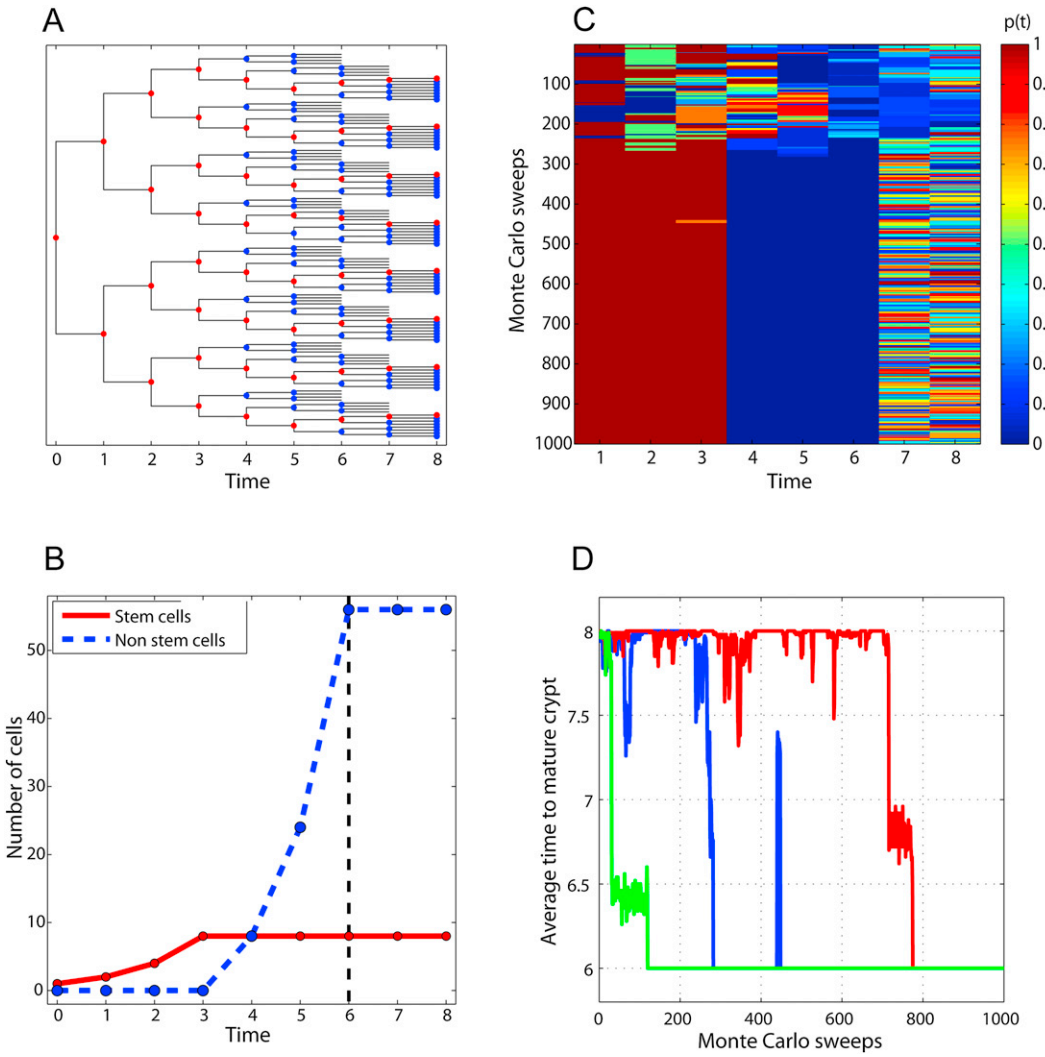

Figure S1. Bang-Bang Control of Symmetric Stem Cell Divisions Remains Optimal When Considering Fixed Life Span of Nonstem Cells, Related to Figure 2

(A) optimal lineage tree in which stem cells (red) first expand for three generations and then switch to asymmetric divisions generating nonstem cells (blue) for the remaining generations. Nonstem cells are extruded after two divisions.

(B) A required crypt size of 8 stem cells and 56 nonstem cells is achieved after 6 generations using the bang-bang control.

(C) Simulated annealing algorithm converges on the optimal bang-bang control solution. Each row shows a stem cell symmetric probability function at different Monte-Carlo sweeps, starting from a random probability function.

(D) Average time to achieve a mature crypt decreases toward the optimal solution as the simulated annealing algorithm proceeds. Shown are three representative iterations, where the blue represents the iteration in (C). All iterations converged on the bang-bang solution of (A and B).

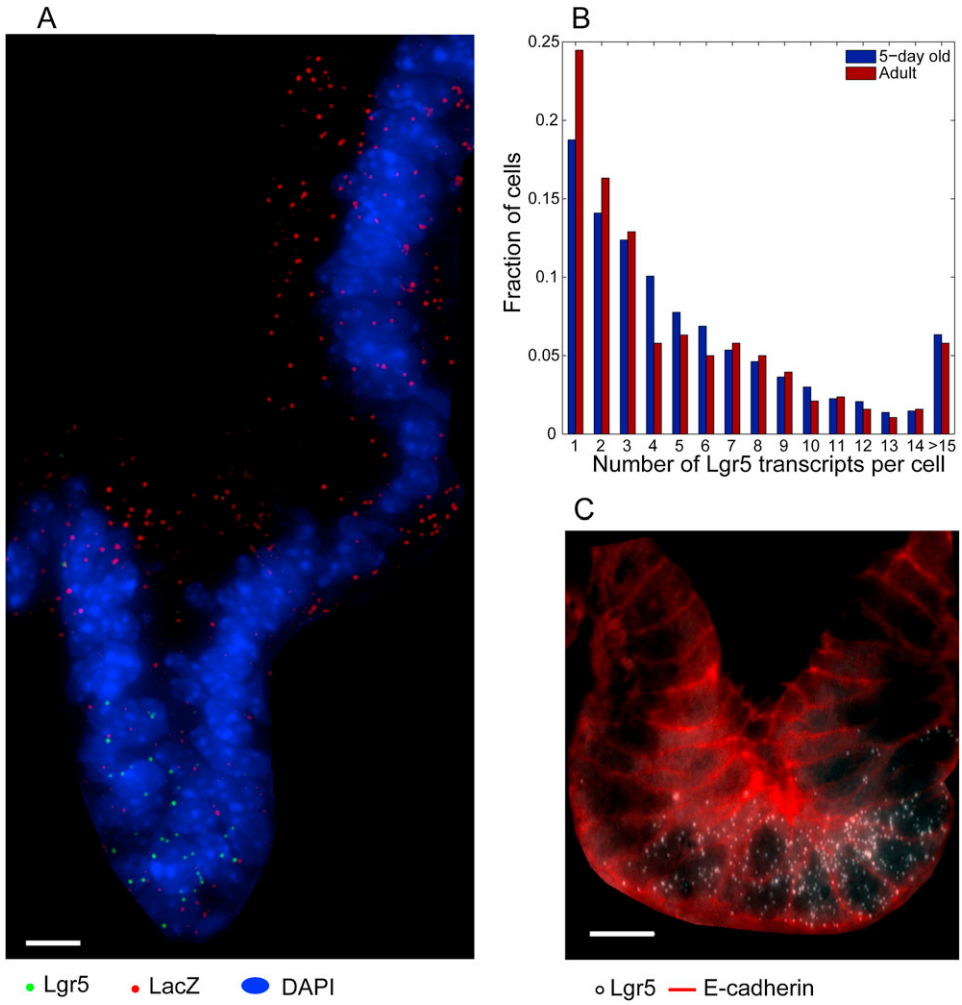

Figure S2. Related to Figure 4

(A) Lgr5 are the stem cells during crypt morphogenesis. Lgr5-Cre/Rosa26-lacZ 5-day old mice injected with tamoxifen and sacrificed 9 days later. Green dots are single Lgr5 transcripts, red dots are lacZ transcripts. Scale bar is 5 microns.

(B) Number of Lgr5 transcripts per cell in infant and adult mice. Quantification based on 6 optical sections spaced 0.3 microns apart.

(C) Single cells were segmented based on immunofluorescense with FITC-E-cadherin antibody which localizes at the cell borders (red). White dots are individual Lgr5 transcripts detected using TMR-labeled single-molecule FISH probes. Scale bar is 10 microns.

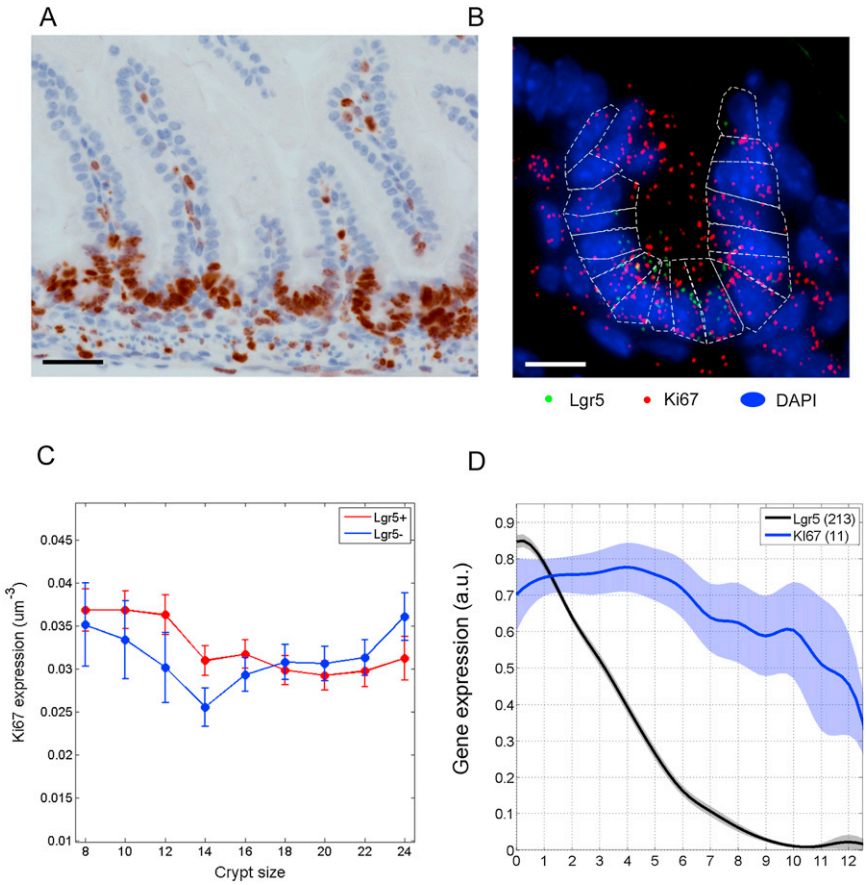

Figure S3. Related to Figure 5

(A) Intestinal crypts in 5-day old mice exhibit a uniform nuclear staining for Ki67 protein. Slide is couterstained with hematoxylin and eosin. Scale bar is 50 microns.
(B) Single-molecule fluorescence in situ co-hybridization for transcripts of Lgr5 (green dots) and the proliferation marker Ki67 (red dots). All dots represent single mRNA molecules. DAPI counterstaining is shown in blue. Segmented cells within the crypt are marked with dashed white lines. Segmentation was based on both DAPI counterstaining and simultaneous immunofluorescense with FITC-E-cadherin antibody which localizes at the cell borders. Scale bar is 10 microns.
(C) Ki67 transcript concentration is similar in Lgr5-positive and Lgr-negative cells and remains constant along the developmental process. Shown are averages of Ki67 expression in single crypt cells versus the sizes of the crypts from which they were sampled along a moving window of +-5 crypt sizes, errorbars are standard errors of the mean.
(D) Lgr5 stem cells are confined to crypt bottoms and are not extruded due to migration. Shown are the mean expression profiles of Lgr5 (black) and Ki67 (blue) at different positions along the crypt axis for duodenal crypts in 5-day old mice. Cell position 0 is the crypt base, profiles for each crypts were obtained by smoothing the profile of transcript concentrations with a moving window of 3 cell positions and dividing by its maximal value in the crypt. Patches are standard errors of the mean. The number of crypts used is shown in parentheses. Lgr5 cells are never found at villi and are confined to lower crypt positions, justifying our assumption that once formed they are not extruded from the crypts.

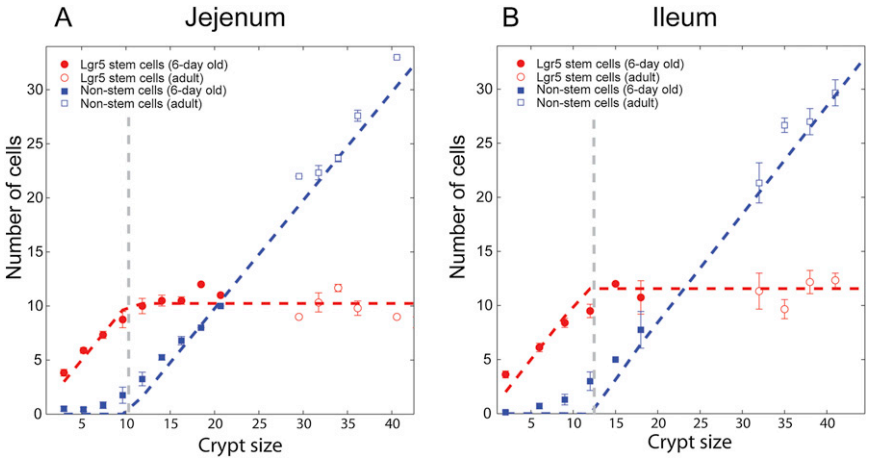

Figure S4. Related to Figure 6

Stem cells in developing crypts in the jejenum (A) and ileum (B) fit the bang-bang control dynamics. Small crypts are exclusively composed of Lgr5 stem cells. When the crypt reaches a size equal to the number of Lgr5 stem cells in the adult crypt (10 cells (in the jejunum) and 12 cells (in the ileum) per crypt longitudinal section, gray vertical dashed line) a transition to nonstem cell production occurs. Dashed red and blue curves are the dynamics predicted from the optimal control solution.